Title	Estimation of vent radii from video recordings and infrasound data analysis: Implications for Vulcanian eruptions from Sakurajima volcano, Japan
Author(s)	Muramatsu, Dan; Aizawa, Koki; Yokoo, Akihiko; Iguchi, Masato; Tameguri, Takeshi
Citation	Geophysical Research Letters (2018), 45(23): 12829-12836
Issue Date	2018-12-18
URL	http://hdl.handle.net/2433/242289
Right	An edited version of this paper was published by AGU. Copyright 2018 American Geophysical Union.
Type	Journal Article
Textversion	publisher

Geophysical Research Letters

RESEARCH LETTER
10.1029/2018GL079898

Key Points:
- Vent radius is estimated by video recordings and infrasound data analysis
- Long-term changes in vent radius were observed over 3.5 years
- A gas-rich zone beneath the vent has a maximum vertical extent of 120 m, assuming it has a cylindrical shape

Supporting Information:
- Supporting Information S1
- Movie S1
- Movie S2
- Movie S3

Correspondence to:
K. Aizawa,
aizawa@sevo.kyushu-u.ac.jp

Citation:
Muramatsu, D., Aizawa, K., Yokoo, A., Iguchi, M., & Tameguri, T. (2018). Estimation of vent radii from video recordings and infrasound data analysis: Implications for Vulcanian eruptions from Sakurajima volcano, Japan. *Geophysical Research Letters*, *45*, 12,829–12,836. https://doi.org/10.1029/2018GL079898

Received 3 AUG 2018
Accepted 18 NOV 2018
Accepted article online 26 NOV 2018
Published online 13 DEC 2018

Estimation of Vent Radii From Video Recordings and Infrasound Data Analysis: Implications for Vulcanian Eruptions From Sakurajima Volcano, Japan

Dan Muramatsu[1], Koki Aizawa[2], Akihiko Yokoo[3], Masato Iguchi[4], and Takeshi Tameguri[4]

[1]Department of Earth and Planetary Sciences, Graduate School of Science, Kyushu University, Fukuoka, Japan, [2]Institute of Seismology and Volcanology, Kyushu University, Fukuoka, Japan, [3]Aso Volcanological Laboratory, Institute for Geothermal Sciences, Graduate School of Science, Kyoto University, Kumamoto, Japan, [4]Sakurajima Volcano Research Center, Disaster Prevention Research Institute, Kyoto University, Kagoshima, Japan

Abstract We estimated the vent radius within Showa Crater of Sakurajima volcano from ejection velocity and flow rate of gas-particle mixtures. The ejection velocity was calculated from video recordings, and the flow rate and volume from infrasound data. Based on the assumption that the vent shape does not change during an explosion, the vent radius was estimated from 201 impulsive Vulcanian eruptions at Showa Crater, yielding values of 6.4–42.3 m (median 23.8 m), which is comparable with the width of fresh lava capping the vent, as photographed from a helicopter. Long-term changes in vent radius (i.e., over several months) show a relationship with magma accumulation within a reservoir 2–5 km beneath the crater. If the top of the conduit is assumed to be cylindrical, then the vertical extent of the gas-rich zone is estimated to be 120 m, which may reflect the depth of gas accumulation and buildup of significant overpressure.

Plain Language Summary A volcanic *vent* is a hole through which ash and volcanic bombs are ejected during an eruption. Beneath the vent, a gas-rich pressurized chamber often forms, particularly before cannon-like explosions. Observing the vent is commonly difficult because of increasing danger when approaching the crater. Accordingly, we present a method to estimate the vent size using eruption videos and infrasound data collected away from the crater. This method was applied to eruptions from Showa Crater of Sakurajima volcano in Japan. The estimated vent size is similar to the actual vent size, as observed from a helicopter. Interestingly, the size of the vent changed over time, increases/decreases in vent size were synchronous with phases of ground deformation, suggesting that the vent size is related to the rate of magma accumulation within the reservoir. The results enhance our understanding of volcanic eruption mechanisms.

1. Introduction

Volcanic eruptions expel mixtures of gas and tephra from a volcanic vent. The size of the vent can provide an indication of the nature of the eruption. For example, the vent radius is one of the parameters that controls eruption column dynamics (Koyaguchi et al., 2010) or the occurrence of monotonic infrasound tremors (Goto & Johnson, 2011). Furthermore, 3-D numerical simulations indicate that vent size is also an important parameter in eruption column collapse (Suzuki & Koyaguchi, 2012). In open-vent volcanoes, the vent size can be directly observed from a location close to the crater (e.g., Johnson et al., 2018), but it is difficult to make such observations because of the associated risks. It is possible to observe the vent by using a helicopter or an unmanned aerial vehicle, but making repeat observations in this way (e.g., for monitoring purposes) is not feasible.

Here we estimate the vent size of active volcanoes by the joint analysis of video recordings and infrasound data. We apply this method to 201 Vulcanian eruptions from Showa Crater of Sakurajima volcano, which is one of the most active volcanoes in Japan. During the observation period (December 2011 to September 2015), Vulcanian eruptions, which explosively erupt gas and ash, occurred repeatedly from Showa Crater.

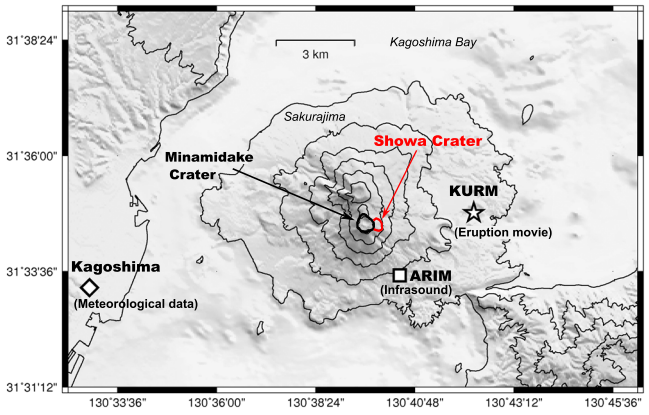

Figure 1. Location of Showa Crater, observation sites on Sakurajima volcano, and the Kagoshima Meteorological Observatory. Contour interval is 200 m. Eruption movies and infrasound data are collected from Kurokami Station (KURM) and Arimura Station (ARIM), respectively.

We estimated the vent size of the crater and the vertical extent of a gas-rich zone (e.g., Iguchi et al., 2008; Ishihara, 1985; Woods, 1995) that formed beneath the vent and caprock, prior to a Vulcanian eruption. The results show changes in the vent size over time, which have implications for magma dynamics within the conduit.

2. Data

2.1. Eruption Movies

Eruption videos used for analysis were taken by a high-sensitivity camera (Hitachi KP-DE500, Hitachi Kokusai Electric) installed at Kurokami Station (KURM) of Kyoto University, 3.5 km east of Showa Crater (Figure 1). The GPS time-synchronized eruption movies were captured continuously and recorded in a hard disk drive at normal speed (i.e., 30 frames per second; Aizawa et al., 2016). The movies were taken between December 2011 and September 2015, when Sakurajima volcano was active, with numerous Vulcanian eruptions from Showa Crater (Figures 1 and 2a). We selected 201 eruption movies that clearly recorded the ejection of a volcanic cloud. Since the viewing angle was identical for all movies, the velocity of the ejecta could be accurately compared. Due to issues with the equipment, there are no data for the periods 22 August to 31 October 2012 and 31 May to 16 August 2014.

2.2. Infrasound Data

Infrasound data were collected from Arimura Station (ARIM), 2.1 km southeast of Showa Crater (Figure 1). The propagation distance from the crater to ARIM is 2.3 km. Time series data were recorded continuously using a low-frequency microphone (Type 7144, ACO) with a frequency range of 0.1–100 Hz, a sampling frequency of 200 Hz, and a 24-bit resolution logger (Iguchi et al., 2013). The observed infrasound waveforms typically show an N-shaped signal with an impulsive compression phase and a subsequent rarefaction phase and long-period coda, similar to the waveforms observed for Vulcanian eruptions from other volcanoes (Johnson & Ripepe, 2011; Morrissey & Chouet, 1997).

3. Methods

3.1. Eruption Movie Analysis

We estimated the ejection velocity of the volcanic cloud from the eruption movies. First, we read the time information for t_1 and t_2 to an accuracy of 0.03 s by sight. Time t_1 represents the point at which a volcanic cloud appears across the eastern rim (front) of the crater (i.e., location I in Figure 2). Time t_2 represents the point at which the volcanic cloud reaches the same altitude as the lowest part of the western rim of the crater (i.e., location II in Figure 2). Second, we assessed the height difference (h) between locations I and II to calculate the ejection velocity as $u \cong h/(t_2 - t_1)$ m/s (Figure 2b). Note that h is the height of the vertical plane above the vent. Since h decreased slightly over 3.5 years due to erosion of the west rim, we used the h value from 26 July 2012. At that time, h measured from a movie image was 16 pixels (between locations I and II in Figure 2), equating to ~45 m, with an uncertainty of ±2.8 m per pixel. Details of the methodology are provided in the supporting information (Text S1).

3.2. Infrasound Analysis

We used infrasound time series data to estimate the volume and flow rate of the ejecta (volcanic cloud) based on a simple acoustic source model (Johnson, 2003; Johnson & Miller, 2014). The model did not consider nonlinear shock wave propagation. Visible shock waves (Yokoo et al., 2013) were observed at Showa Crater, but this nonlinear phenomenon is too complicated to be considered without numerical modeling (e.g., Morrissey & Chouet, 1997). N-shaped infrasound signals produced by volcanic explosions (Figure 2c) are modeled using a simple acoustic source (e.g., a monopole source). Assuming a half-space and 1-D propagation of the acoustic signal, which is dependent on distance (r), the overpressure (δp) at any distance from the vent is as follows (Lighthill, 1978):

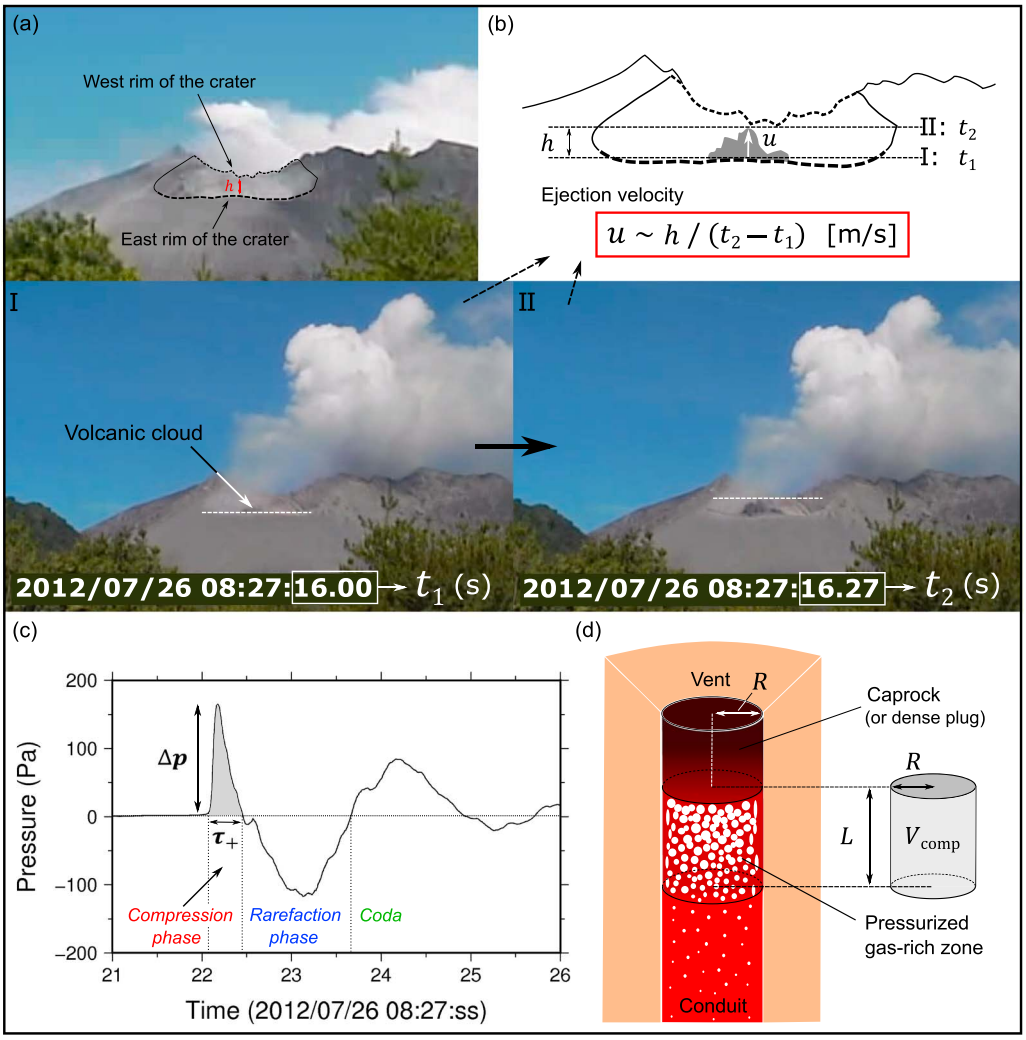

Figure 2. Summary of the analytical methods employed in this study. (a) Showa Crater, photographed from Kurokami (KURM). (b) Calculation of the apparent ejection velocity of the volcanic cloud. Times t_1 (I) and t_2 (II) are taken from video recordings. The ejection velocity is calculated by dividing the height difference between location I and II (h) by the time difference ($t_2 - t_1$ s). (c) Infrasound waveform of the eruption (I and II). This study focuses on the first impulsive compression phase (gray region) of the analysis. (d) Model of the vent and the gas-rich zone. Radius R and vertical extent L are estimated assuming a cylindrical conduit. In this case, R is equal to the vent radius.

$$\delta p(t,r) = \frac{\rho_a}{2\pi r}\ddot{V}(t - r/c) \tag{1}$$

where $\ddot{V}(t)$ is the volume acceleration of ejecta, c is the atmospheric sound velocity, and ρ_a is the atmospheric density. When material is ejected from a volcanic vent, equivalent displacement of the atmosphere occurs above the vent, generating excess pressure by the same amount as the volume acceleration of the ejecta. Calculating equation (1) for a given time allows the volume flow rate $\dot{V}(t)$ of ejecta to be determined as follows (e.g., Johnson & Miller, 2014; Yamada et al., 2017):

$$\dot{V}(t) = \frac{2\pi r}{\rho_a}\int \delta p(t,r)\mathrm{d}t \tag{2}$$

In the present analysis, we only focus on the first impulsive compression phase (Figure 2c) because the subsequent rarefaction phase and coda may be excited by diffraction and reflection during propagation (path effects) rather than the source conditions (Fee et al., 2017; Kim et al., 2015). The first compression phase is directly related to overpressure of the gas-rich zone within the conduit (Morrissey & Chouet, 1997). By

setting the arrival time to zero and the duration of the compression phase to τ_+, the volume flow rate of the compression phase ($\dot{V}_{max}$) was estimated as follows:

$$\dot{V}_{max} = \frac{2\pi r}{\rho_a} \int_0^{\tau_+} \delta p(t, r) \mathrm{d}t \tag{3}$$

A short *preceding phase* is sometimes observed before the first compression phase (Yokoo et al., 2009, 2013). Setting the arrival time to zero means that the preceding phase was excluded. The volume of the compression phase (V_{comp}; i.e., the volume of the gas-rich zone) was estimated by calculating equation (3) at a given t, from 0 to τ_+, as follows:

$$V_{comp} = \frac{2\pi r}{\rho_a} \iint_0^{\tau_+} \delta p(t, r) \mathrm{d}t^2 \tag{4}$$

The maximum volume flow rate (m^3/s) and volume (m^3) of the gas-rich zone were estimated for each eruption. The atmospheric density (ρ_a) was calculated at an altitude of 650 m (i.e., at the base of Showa Crater) from temperature and atmospheric pressure data collected at the Kagoshima Meteorological Observatory (the closest observation site to Sakurajima; Figure 1) at the time of the eruption. Time series data processing did not involve waveform conditioning, as proposed by Johnson and Miller (2014), but its effect would have been negligible because the amplitude of the first compression phase was large. As compressibility of gas was ignored, the estimated volume is the maximum possible value.

In this study, we interpret the gas-rich zone to comprise a highly vesiculated and pressurized magma (Figure 2d), rather than a chamber filled solely with gas. Vulcanian eruptions from Sakurajima volcano are frequent, occasionally occurring every few minutes (see supporting information). It seems unlikely that the gas-filled space would form over such a short timescale. The *gas-rich zone* referred to in this study corresponds to the *gas chamber* (Ishihara, 1985) and *gas pocket* (e.g., Iguchi et al., 2008; Maryanto et al., 2008; Tameguri et al., 2002; Yokoo et al., 2009, 2013) described in previous studies of Vulcanian eruptions from Sakurajima volcano.

3.3. Estimation of Vent Radius

We present a simple method for estimation of the vent size by combining two independent observations (i.e., video recordings and infrasound data). Assuming a circular vent with radius R, the relationship between the volume flow rate and ejection velocity from the vent is as follows:

$$\dot{V}(t) = \pi R^2 u(t) \tag{5}$$

Equation (5) assumes that the vent radius remained constant during each eruption and that the time at which u was measured corresponds to the time at which the volume velocity was at its maximum ($\dot{V}_{max}$). The third assumption is that equation (5) approximates the natural conditions, since $\dot{V}(t)$ converges to a constant value at the end of the initial compression phase (Figure 2c and equation (2)), at which point u is also estimated. Based on these assumptions, equation (5) can be rewritten to give the vent radius as follows:

$$R \sim \sqrt{\frac{\dot{V}_{max}}{\pi u}} \tag{6}$$

We also estimated the vertical extent of the gas-rich zone (L) located beneath the vent. Assuming that the top of the conduit is cylindrical and that R is equal to the radius of the gas-rich zone (Figure 2d), L can be estimated by dividing the volume (V_{comp}) of the gas-rich zone by the cross-sectional area (πR^2) of the vent:

$$L \sim \frac{V_{comp}}{\pi R^2} \tag{7}$$

This equation is only valid if the discharge rate from the gas-rich zone is much larger than the charging rate from the magma body within the conduit. We analyzed the first compression phase, which occurred

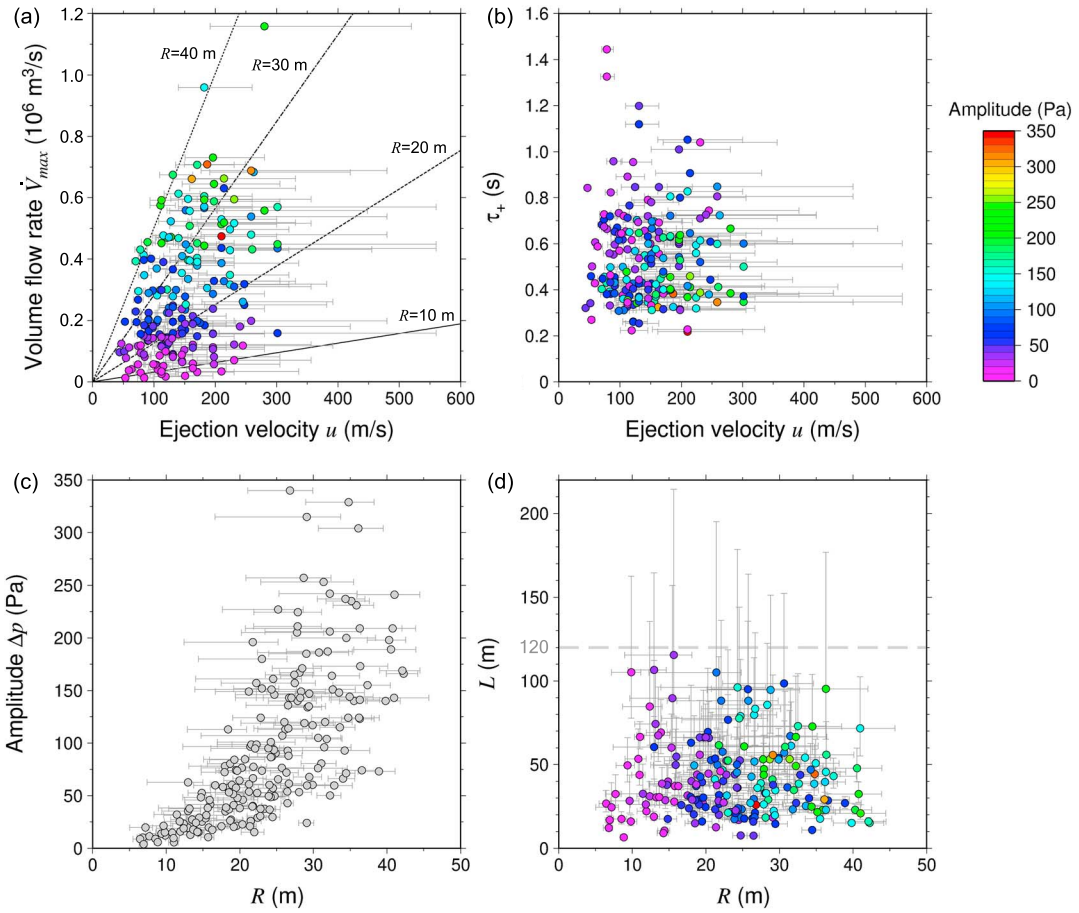

Figure 3. Relationships between the estimated parameters. The symbol colors in (a), (b), and (d) reflect the maximum amplitude of the first compression phase (Δp in Figure 2c) of each event. Gray error bars represent maximum and minimum values for u, R, and L based on the $t_2 - t_1$ uncertainty. (a) Plot of ejection velocity u versus the maximum volume flow rate $\dot{V}_{max}$. The four lines correspond to R = 10, 20, 30, and 40 m and are calculated from equation (5) in the main text. (b) Relationship between the ejection velocity u and duration of the first compression phase τ_+. (c) Relationship between the vent radius (R) and the maximum amplitude of the first compression phase (Δp). (d) Relationship between the vent radius R and the vertical extent L of the gas-rich zone. Maximum L = 120 m is shown by the gray dashed line.

instantaneously due to a rupture in the gas-rich zone. Supplying from the underlying magma body is therefore considered to have negligible effect on the estimation of L.

We evaluate the errors involved in the estimation of R and L. The largest errors arise during estimation of the ejection velocity (u). As the uncertainty associated with the time read from the movies (t_1 and t_2) is 0.03 s, the maximum uncertainty of the time difference $t_2 - t_1$ is 0.06 s. The maximum and minimum values for u, R, and L are based on the $t_2 - t_1$ uncertainty, as shown in Figure 3 (gray error bars). In addition to the above errors, R may have been overestimated by neglecting propagation effects. According to the numerical model of Kim et al. (2015), the use of 1-D acoustic Green's function means that the peak volume flow rate during the first compression phase may have been overestimated by up to 55%, compared with 3-D modeling that considers realistic propagation effects (e.g., local topographic scattering). This corresponds to a 24% overestimation of R.

4. Results and Discussion

4.1. Vent Radius (R)

The estimated vent radius (R) is 6.4–42.3 m (median 23.8 m), which is comparable with the width of red-hot portion of the fresh lava capping the vent, as photographed from a helicopter on 31 May and 11 July 2011 (available at: http://www.data.jma.go.jp/svd/vois/data/tokyo/STOCK/monthly_v-act_doc/fukuoka/2011y/

506_11y.pdf). The red-hot portion of the fresh lava was inferred to represent the vent size at the top of the conduit (Ishihara, 1985). Ejection velocities estimated from the video recordings range between 43.8 and 301.5 m/s. The volume flow rate during the first compression phase was estimated from infrasound data to range between 1.3×10^4 and 1.2×10^6 m^3/s. Figure 3a shows the u–$\dot{V}_{max}$ plot, with lines shown for R = 10, 20, 30, and 40 m. The estimated vent radius R have a large range of values. We found no clear relationship between u and $\dot{V}_{max}$. Figure 3b shows the relationship between u and τ_+. The weak negative correlation indicates that the large ejection velocity u results in the short-lived first compression phase, τ_+, but we also need to take into account the vertical extent of the gas-rich zone to investigate τ_+. Figure 3c shows the relationship between Δp and R, which is discussed in section 4.3.

4.2. Vertical Extent (L) of the Pressurized Gas-Rich Zone

The volume of the gas-rich zone (V_{comp}) was estimated from infrasound data to be 1.6×10^3 to 3.9×10^5 m^3. The estimated extent of the gas-rich zone (L) is 6.6–115.5 m, based on equation (7) and the assumption of a constant cylindrical shape. Figure 3d shows the relationship between R and L. The maximum extent of L was estimated to be ~120 m (gray line in Figure 3d). Note that we treat the duration of the initial compression phase τ_+ as the period of discharge from the gas-rich zone. The maximum velocity of material emitted from the gas-rich zone may be approximated as u. Therefore, L may be approximated as $\frac{1}{2}u{\cdot}\tau_+$. Indeed, this simple method produced values of 7.0–119.9 m, which are similar to L (see supporting information). We suggest that the gas-rich zone formed due to gas exsolution, growth, and pressure accumulation at depths of up to 120 m within the shallow conduit. Significant gas exsolution and accumulation at the top of the conduit is supported by petrological analysis of Vulcanian eruption deposits from the Soufrière Hills volcano, Montserrat (e.g., Burgisser et al., 2010), and Sakurajima volcano (e.g., Miwa & Toramaru, 2013), as well as magma convection models (Kazahaya et al., 1994; Shinohara, 2008).

4.3. Temporal Changes in R

Figure 4 shows temporal changes in infrasound strength, πR^2 (i.e., the cross-sectional area of the vent), R, and ground deformation (tilt). Long-term variations in Δp, R, and πR^2 were observed over several months (red and blue arrows in Figures 4b and 4c). However, τ_+, u, $\dot{V}_{max}$, V_{comp}, and L do not exhibit significant long-term variation (see supporting information). The long-term changes in R and πR^2 cannot be explained by seasonal changes in air temperature or ocean tide because these parameters do not have a significant influence on u or Δp. Alternatively, the temporal changes in R and πR^2 may indicate that our assumptions do not hold true. We assumed that the vent size remained constant during the first compression phase (Figure 2c), but the validity of this assumption remains to be tested. If a strong explosion with a large Δp enlarges the vent over a timescale of 0.1 s, the estimation of R may be influenced by the strength of the eruption. For example, a strong explosion may increase the vent size, thereby reducing u over a short timeframe and resulting in a large estimate of R. The observed positive correlation between Δp and R (Figure 3c) does not contradict this interpretation; however, we infer this mechanism is minor because significant vent opening is required. We suggest that Figure 3c simply indicates that a strong explosion occurs from a large vent.

It is important to consider temporal changes in vent size. Figure 4 shows that changes in R, πR^2, and tilt (crater orientation; Figure 4d), as determined from the Arimura underground tunnel (ARIM), are contemporaneous; crater uplift and subsidence are associated with decreasing and increasing R and πR^2, respectively. The variable tilt over months (red and blue arrows) in 2012 and 2015 are not observed for the period 2007–2011 (see supporting information). Long-term changes in tilt (red and blue arrows in Figure 4d) in the ARIM are interpreted to be a result of inflation and deflation of the magma reservoir at 2–5 km below the crater (Hotta, Iguchi, Ohkura, & Yamamoto, 2016). The vent size may therefore be related to the magma accumulation rate within the reservoir. Assuming that the vent radius is proportional to the radius of the volcanic conduit, it is possible that a small conduit (i.e., small R and πR^2) prevented an efficient discharge of magma, meaning that magma would have accumulated within the reservoir, causing uplift of the crater. On 15 August 2015 (green line in Figure 4c), $1.7–2.7 \times 10^6$ m^3 of magma was emplaced ~1.0–1.8 km beneath Showa Crater, causing numerous volcano-tectonic earthquakes and rapid ground uplift (Hotta, Iguchi, & Tameguri, 2016; Morishita et al., 2016). Prior to the intrusion of magma (period B in Figure 4c), R decreased rapidly compared with previous changes. The average decrease in R during periods A and B was −0.14 and −0.25 m/day, respectively (Figure 4c). We propose that the conduit became blocked during period B and that magma

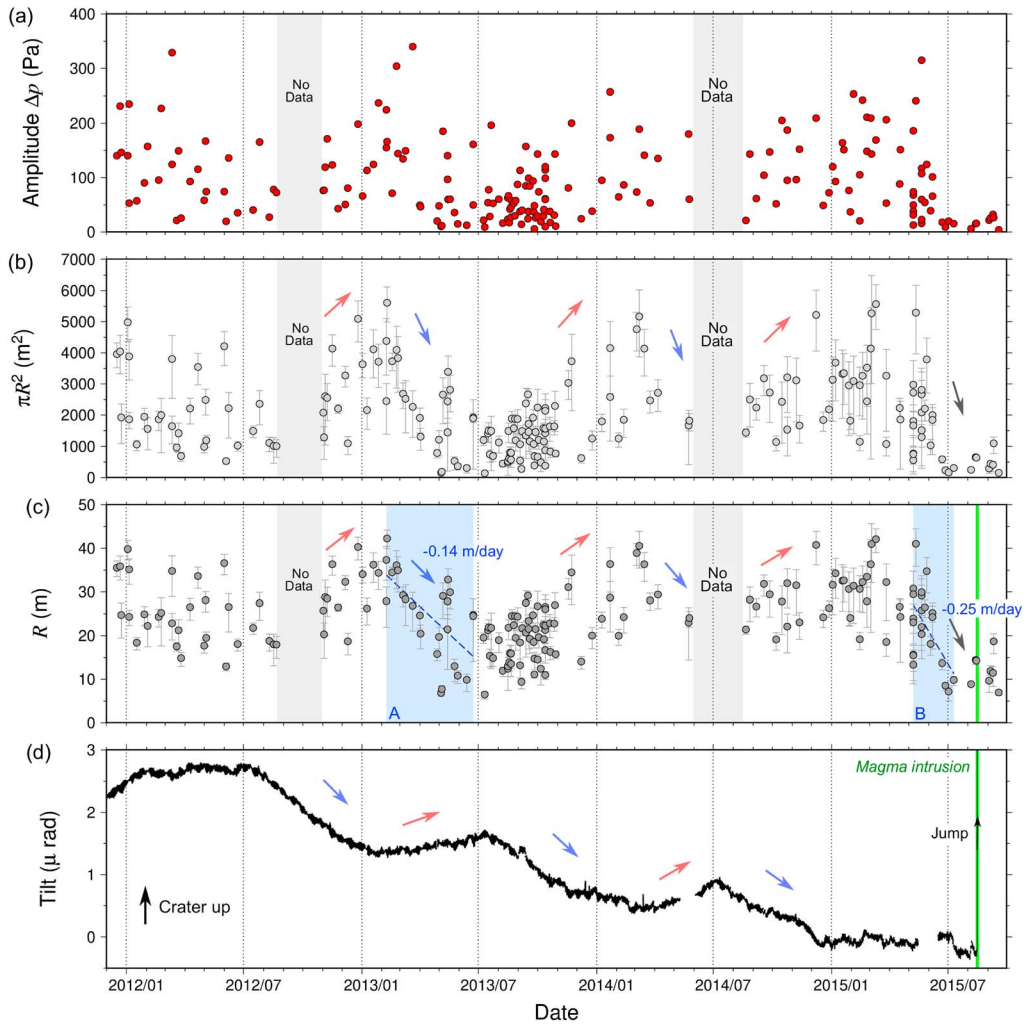

Figure 4. Plots of parameter values over time. Gray error bars represent maximum and minimum values for R and πR^2 based on the $t_2 - t_1$ uncertainty. Gray shaded regions represent data-missing periods. A peak amplitude of the first compression phase (Δp in Figure 2c) of each event. (b) Cross-sectional area πR^2 (m^2) of the estimated vent. The arrows highlight where πR^2 is increasing (red) or decreasing (blue). (c) Variation in the estimated vent radius R. The arrows highlight where R is increasing (red) or decreasing (blue). The green line indicates a magma intrusion event on 15 August 2015 (Hotta, Iguchi, & Tameguri, 2016). Prior to this event, the vent radius rapidly decreased (gray arrow). The average rate of change in R during periods A and B (blue shaded regions) was calculated by linear regression. (d) Variation in tilt (crater orientation) as observed within the Arimura underground tunnel over time. Long-term changes in tilt (red and blue arrows) are consistent with the changes in R and πR^2.

migration occurred along a new route, resulted in intrusion. Conduit choking is also supported by a decrease in SO_2 content at 1 month prior to the magma intrusion (JMA Annual Report, 2015; available at http://www.data.jma.go.jp/svd/vois/data/tokyo/STOCK/monthly_v-act_doc/fukuoka/2015y/506_15y.pdf).

5. Conclusions

We estimated the vent radius of Showa Crater and the vertical extent of a pressurized gas-rich zone by analyzing video recordings and infrasound data. The estimated vent radius ranges between 6.4 and 42.3 m (median 23.8 m), which is comparable with the width of fresh lava that caps the vent, as photographed from a helicopter. We found no relationship between the volume flow rate during the first compression phase ($\dot{V}_{max}$) and ejection velocity of the volcanic cloud. Long-term changes in vent radius (i.e., over several months) were synchronized with the tilt record (crater orientation), and crater uplift and subsidence were associated with decreasing and increasing R, respectively. The maximum vertical extent of the gas-rich zone is 120 m, suggesting that exsolved gas accumulation and significant overpressure buildup occur at depths of 0 to

120 m beneath the magma cap, near the top of the conduit. Our quantitative results constrain the pre-eruption conditions at the top of the conduit of Showa Crater.

Acknowledgments
We thank H. Shimizu and T. Kozono for insightful discussions. We thank the Japan Meteorological Agency and Japanese Ministry of Land, Infrastructure, Transport, and Tourism (MLIT). Meteorological data from Kagoshima City were collected at 10-min intervals by the Japan Meteorological Agency (JMA). Infrasound data were provided by the Osumi Office of the River and National Highway, MLIT. Constructive comments from two anonymous reviewers and Associate Editor R. Carey have greatly improved the manuscript. Data used in this study are available from the following website: https://archive.iii.kyushu-u.ac.jp/public/vYWMgAHI0o5ARGYBzShmrCYuDheen-jx_rTinBCOKnAAp. This work was funded by MEXT KAKENHI (grant JP23740332). D. M. was supported by the MEXT Integrated Program for Next Generation Volcano Research and Human Resource Development.

References

Aizawa, K., Cimarelli, C., Alatorre-Ibargüengoitia, A. M., Yokoo, A., Dingwell, D. B., & Iguchi, M. (2016). Physical properties of volcanic lightning: Constraints from magnetotelluric and video observations at Sakurajima volcano, Japan. *Earth and Planetary Science Letters*, *444*, 45–55. https://doi.org/10.1016/j.epsl.2016.03.024

Burgisser, A., Poussineau, S., Arbaret, L., Druitt, T. H., Giachetti, T., & Bourdier, J. L. (2010). Pre-explosive conduit conditions of the 1997 Vulcanian explosions at Soufriere Hills Volcano, Montserrat: I. Pressure and vesicularity distributions. *Journal of Volcanology and Geothermal Research*, *194*(1–3), 27–41. https://doi.org/10.1016/j.jvolgeores.2010.04.008

Fee, D., Izbekov, P., Kim, K., Yokoo, A., Lopez, T., Prata, F., et al. (2017). Eruption mass estimation using infrasound waveform inversion and ash and gas measurements: Evaluation at Sakurajima Volcano, Japan. *Earth and Planetary Science Letters*, *480*, 42–52. https://doi.org/10.1016/j.epsl.2017.09.043

Goto, A., & Johnson, J. B. (2011). Monotonic infrasound and Helmholtz resonance at Volcan Villarrica (Chile). *Geophysical Research Letters*, *38*, L06301. https://doi.org/10.1029/2011GL046858

Hotta, K., Iguchi, M., Ohkura, T., & Yamamoto, K. (2016). Multiple-pressure-source model for ground inflation during the period of high explosivity at Sakurajima volcano, Japan - combination analysis of continuous GNSS, tilt and strain data. *Journal of Volcanology and Geothermal Research*, *310*, 12–25. https://doi.org/10.1016/j.jvolgeores.2015.11.017

Hotta, K., Iguchi, M., & Tameguri, T. (2016). Rapid dike intrusion into Sakurajima volcano on August 15, 2015, as detected by multi-parameter ground deformation observations. *Earth, Planets and Space*, *68*(1), 1–9. https://doi.org/10.1186/s40623-016-0450-0

Iguchi, M., Tameguri, T., Ohta, Y., Ueki, S., & Nakao, S. (2013). Characteristics of volcanic activity at Sakurajima Volcano's Showa crater during the period 2006 to 2011. *Bulletin of the Volcanological Society of Japan*, *58*(1), 115–135. https://doi.org/10.18940/kazan.58.1_115

Iguchi, M., Yakiwara, H., Tameguri, T., Hendrasto, M., & Hirabayashi, J. I. (2008). Mechanism of explosive eruption revealed by geophysical observations at the Sakurajima, Suwanosejima and Semeru volcanoes. *Journal of Volcanology and Geothermal Research*, *178*(1), 1–9. https://doi.org/10.1016/j.jvolgeores.2007.10.010

Ishihara, K. (1985). Dynamical analysis of volcanic explosion. *Journal of Geodynamics*, *3*(3–4), 327–349. https://doi.org/10.1016/0264-3707(85)90041-9

Johnson, J. B. (2003). Generation and propagation of infrasonic airwaves from volcanic explosions. *Journal of Volcanology and Geothermal Research*, *121*(1–2), 1–14. https://doi.org/10.1016/S0377-0273(02)00408-0

Johnson, J. B., & Miller, A. J. C. (2014). Application of the monopole source to quantify explosive flux during Vulcanian explosions at Sakurajima Volcano (Japan). *Seismological Research Letters*, *85*, 1163–1176. https://doi.org/10.1785/0220140058

Johnson, J. B., & Ripepe, M. (2011). Volcano infrasound: A review. *Journal of Volcanology and Geothermal Research*, *206*(3–4), 61–69. https://doi.org/10.1016/j.jvolgeores.2011.06.006

Johnson, J. B., Watson, L. M., Palma, J. L., Dunham, E. M., & Anderson, J. F. (2018). Forecasting the eruption of an open-vent volcano using resonant infrasound tones. *Geophysical Research Letters*, *45*, 2213–2220. https://doi.org/10.1002/2017gl076506

Kazahaya, K., Shinohara, H., & Saito, G. (1994). Excessive degassing of Izu-Oshima volcano: Magma convection in a conduit. *Bulletin of Volcanology*, *56*(3), 207–216. https://doi.org/10.1007/s004450050029

Kim, K., Fee, D., Yokoo, A., & Lees, J. M. (2015). Acoustic source inversion to estimate volume flux from volcanic explosions. *Geophysical Research Letters*, *42*, 5243–5249. https://doi.org/10.1002/2015gl064466

Koyaguchi, T., Suzuki, Y. J., & Kozono, T. (2010). Effects of the crater on eruption column dynamics. *Journal of Geophysical Research*, *115*, B07205. https://doi.org/10.1029/2009JB007146

Lighthill, M. J. (1978). *Waves in fluids* (p. 504). Cambridge, UK: Cambridge University Press.

Maryanto, S., Iguchi, M., & Tameguri, T. (2008). Constraints on the source mechanism of harmonic tremors based on seismological, ground deformation, and visual observations at Sakurajima volcano, Japan. *Journal of Volcanology and Geothermal Research*, *170*(3–4), 198–217. https://doi.org/10.1016/j.jvolgeores.2007.10.004

Miwa, T., & Toramaru, A. (2013). Conduit process in Vulcanian eruptions at Sakurajima volcano, Japan: Inference from comparison of volcanic ash with pressure wave and seismic data. *Bulletin of Volcanology*, *75*(1), 685. https://doi.org/10.1007/s00445-012-0685-y

Morishita, Y., Kobayashi, T., & Yarai, H. (2016). Three-dimensional deformation mapping of a dike intrusion event in Sakurajima in 2015 by exploiting the right- and left-looking ALOS-2 InSAR. *Geophysical Research Letters*, *43*, 4197–4204. https://doi.org/10.1002/2016gl068293

Morrissey, M. M., & Chouet, B. A. (1997). Burst conditions of explosive volcanic eruptions recorded on microbarographs. *Science*, *275*(5304), 1290–1293. https://doi.org/10.1126/science.275.5304.1290

Shinohara, H. (2008). Excess degassing from volcanoes and its role on eruptive and intrusive activity. *Reviews of Geophysics*, *46*, RG4005. https://doi.org/10.1029/2007RG000244

Suzuki, Y. J., & Koyaguchi, T. (2012). 3-D numerical simulations of eruption column collapse: Effects of vent size on pressure-balanced jet/plumes. *Journal of Volcanology and Geothermal Research*, *221-222*, 1–13. https://doi.org/10.1016/j.jvolgeores.2012.01.013.

Tameguri, T., Iguchi, M., & Ishihara, K. (2002). Mechanism of explosive eruptions from moment tensor analyses of explosion earthquakes at Sakurajima volcano. Japan. *Bulletin of the Volcanological Society of Japan*, *47*, 197–215.

Woods, A. W. (1995). A model of vulcanian explosions. *Nuclear Engineering and Design*, *155*, 345–357.

Yamada, T., Aoyama, H., Nishimura, T., Iguchi, M., & Hendrasto, M. (2017). Volcanic eruption volume flux estimations from very long period infrasound signals. *Geophysical Research Letters*, *44*, 143–151. https://doi.org/10.1002/2016gl071047

Yokoo, A., Iguchi, M., Tameguri, T., & Yamamoto, K. (2013). Processes prior to outburst of Vulcanian eruption at Showa crater of Sakurajima volcano. *Bulletin of the Volcanological Society of Japan*, *58*, 163–181. https://doi.org/10.18940/kazan.58.1_163

Yokoo, A., Tameguri, T., & Iguchi, M. (2009). Swelling of a lava plug associated with a Vulcanian eruption at Sakurajima volcano, Japan, as revealed by infrasound record: Case study of the eruption on January 2, 2007. *Bulletin of Volcanology*, *71*(6), 619–630. https://doi.org/10.1007/s00445-008-0247-5